

Article

Cu₂S Nanoflakes Decorated with NiS Nanoneedles for Enhanced Oxygen Evolution Activity

Le Wang^{1,2}, Mancong Li^{1,2}, Yingxin Lyu², Jiawen Liu², Jimin Du^{1,2,*}  and Dae Joon Kang^{3,*}

¹ College of Chemistry and Molecular Engineering, Zhengzhou University, Zhengzhou 450001, China; wl3200852214@163.com (L.W.); lmc1234562022@163.com (M.L.)

² School of Chemistry and Chemical Engineering, Anyang Normal University, Anyang 455002, China; l2801106022@163.com (Y.L.); l718372708@163.com (J.L.)

³ Department of Physics, Sungkyunkwan University, 2066, Seobu-ro, Jangan-gu, Suwon 16419, Gyeonggi-do, Korea

* Correspondence: djm@iccas.ac.cn (J.D.); dj kang@skku.edu (D.J.K.)

Abstract: Metal sulfides are considered excellent materials for oxygen evolution reaction because of their excellent conductivity and high electrocatalytic activity. In this report, the NiS-Cu₂S composites were prepared on copper foam (NiS-Cu₂S-CF) using a facile synthetic strategy. The scanning electron microscopy results confirmed that the NiS nanoneedles were successfully grown on Cu₂S nanoflakes, greatly increasing the active sites. Particularly, the optimized 15% NiS-Cu₂S-CF composite demonstrated excellent oxygen evolution activity with a small overpotential of 308 mV@20 mA cm⁻², which is significantly smaller than that of noble metal-based electrocatalysts and other NiS-Cu₂S-CF composites. The enhanced oxygen evolution activity is attributed to the unique morphology that can provide ample active sites, rich ion-transfer pathways, and the synergistic effect between NiS and Cu₂S, which can boost the electron transfer rate.

Keywords: NiS; Cu₂S; electrocatalysts; oxygen evolution reaction



Citation: Wang, L.; Li, M.; Lyu, Y.; Liu, J.; Du, J.; Kang, D.J. Cu₂S Nanoflakes Decorated with NiS Nanoneedles for Enhanced Oxygen Evolution Activity. *Micromachines* **2022**, *13*, 278. <https://doi.org/10.3390/mi13020278>

Academic Editor: Hong Li

Received: 13 January 2022

Accepted: 8 February 2022

Published: 9 February 2022

Publisher's Note: MDPI stays neutral with regard to jurisdictional claims in published maps and institutional affiliations.



Copyright: © 2022 by the authors. Licensee MDPI, Basel, Switzerland. This article is an open access article distributed under the terms and conditions of the Creative Commons Attribution (CC BY) license (<https://creativecommons.org/licenses/by/4.0/>).

1. Introduction

Nowadays, precious metal-based materials, including RuO₂ and IrO₂, are considered excellent electrocatalysts for oxygen evolution reactions (OER) [1,2]. However, their scarcity and high cost prevent them from being used on a large scale. Hence, the development of earth-abundant, low-cost, high-performance catalysts to replace precious-metal-based electrocatalysts has become critical. Because of their high electrical conductivity, excellent catalytic performance, ease of synthesis, and low cost, metal sulfide-based materials have received much attention [3–8]. Of the various metal sulfides, Cu₂S is considered a potential material for oxygen evolution because of its distinct morphology, good conductivity, and high catalytic performance [9–11]. Many researchers have prepared Cu₂S and its composites for OER [12–15]. However, the OER activities of the Cu₂S-based materials are still poor compared to those of precious metal-based materials.

Meanwhile, NiS has recently been demonstrated to be an excellent cocatalyst for oxygen evolution because of its good chemical and physical properties [16–18]. Furthermore, the construction of binary metal sulfides heterostructure is a promising route for significantly improving the OER activity of catalysts because the heterostructure can enhance charge transfer and provides more surface-active sites [19–21]. For instance, Li et al. fabricated the NiS/Bi₂WO₆ heterostructure for OER, which exhibited a small overpotential of 527 mV@10 mA cm⁻² [22]. Luo et al. synthesized the NiS/C₃N₄ composites for oxygen evolution, which displayed a small overpotential of 334 mV@10 mA cm⁻² [23]. Jiang et al. constructed a NiS/Fe₃O₄ composite with a small overpotential of 310 mV@10 mA cm⁻² for OER [24]. As a result, taking into account the exceptional catalytic performance of the NiS, we attempted to integrate the NiS with Cu₂S to construct NiS-Cu₂S heterostructure,

which could be an efficient strategy for increasing the OER activity of the Cu_2S . Hence, we rationally designed NiS nanoneedles on Cu_2S nanoflakes as an efficient OER electrocatalyst, which has not yet been reported.

In addition, electrocatalysts grown on 3D porous copper foam (CF) can provide not only a large surface area but also abundant ion-transfer pathways in the OER process. Hence, we employed CF as a 3D porous template substrate in this work. The NiS- Cu_2S composites were prepared on CF (NiS- Cu_2S -CF) using a facile synthetic route. The scanning electron microscopy (SEM) images demonstrated that the NiS nanoneedles were successfully grown on Cu_2S nanoflakes, providing a large number of active surface sites. The electrochemical measurement results indicated that the optimized 15% NiS- Cu_2S -CF electrocatalysts exhibited an outstanding OER activity of 308 mV at 20 mA cm^{-2} in a 1 M KOH electrolyte, which is much higher than that of RuO_2 -based electrocatalysts (350 mV at 20 mA cm^{-2}). These results suggest that the NiS- Cu_2S -CF composite be a candidate for oxygen evolution.

2. Materials and Methods

Fabrication of NiS- Cu_2S heterostructure on CF: the NiS- Cu_2S heterostructure was prepared through a facial synthetic route combined with electrochemical-corrosion and hydrothermal reaction methods. More detailed information about the preparation process, materials characterizations, and electrocatalytic performance test are provided in Supporting Information.

3. Results

The fabrication process of the NiS- Cu_2S -CF composites is given in the following section. Firstly, the Cu_2O was fabricated on CF using the electrochemical-corrosion method; then, the Cu_2S -CF was formed by the sulfidation of Cu_2O -CF; finally, the NiS was grown on Cu_2S -CF by a facile hydrothermal method. More detailed information on the fabrication process is shown in Supporting Materials. To improve the OER performance of the sample, we tuned the molar ratios of Ni and Cu in the NiS- Cu_2S -CF composites. The effects of molar ratios of Ni and Cu in the NiS- Cu_2S -CF composites were investigated through an inductively coupled plasma atomic emission spectrometer (ICP-AES). The result is displayed in Table S1 (Supporting Materials). The SEM was employed to examine the morphology of the as-prepared products. Figure S1 (Supporting Materials) show the SEM images of the CF and Cu_2O -CF. Figure S2 (Supporting Materials) shows the SEM image of Cu_2S -CF composites, indicating that the nanoflake-shaped Cu_2S were successfully grown on CF. Such morphology can offer a large number of growth sites for NiS. Figure S3 (Supporting Materials) presents the SEM image of NiS-CF composites showing the NiS with nanoneedles were successfully decorated on CF. The SEM images of the NiS- Cu_2S -CF composites are shown in Figure 1. As shown, when the molar ratio of the Ni ions was 5%, the surface of the Cu_2S nanoflakes was found to be decorated with a limited amount of NiS nanoneedles (Figure 1a–c). When the molar ratio of the Ni ions approached 10% and 15%, numerous NiS nanoneedles were uniformly grown on the Cu_2S surface (Figure 1d–i). The length and diameter of the NiS nanoneedles were 40 and 10 nm, respectively. Furthermore, as the molar ratio of the Ni ions reaches 20%, the size of NiS decreased, possibly because a large amount of the Ni ions affected the length of the NiS nanoneedles (Figure 1j–l). Here, we also propose a plausible formation mechanism on how the NiS nanoneedles were formed on Cu_2S nanoflakes; once Ni ions were evenly distributed on the surface of Cu_2S nanoflakes, a large amount of NiS nuclei were formed on the Cu_2S nanoflakes during the hydrothermal process. NiS nanoneedles were successfully grown on Cu_2S nanoflakes with an increase in reaction time. It should be noted that the Cu_2S nanoflakes decorated with NiS nanoneedles can not only provide numerous surface active sites, but can also offer more contact areas between electrodes and electrolytes during the oxygen evolution process.

Modifying the molar ratios of the Ni ions in NiS-Cu₂S-CF composites

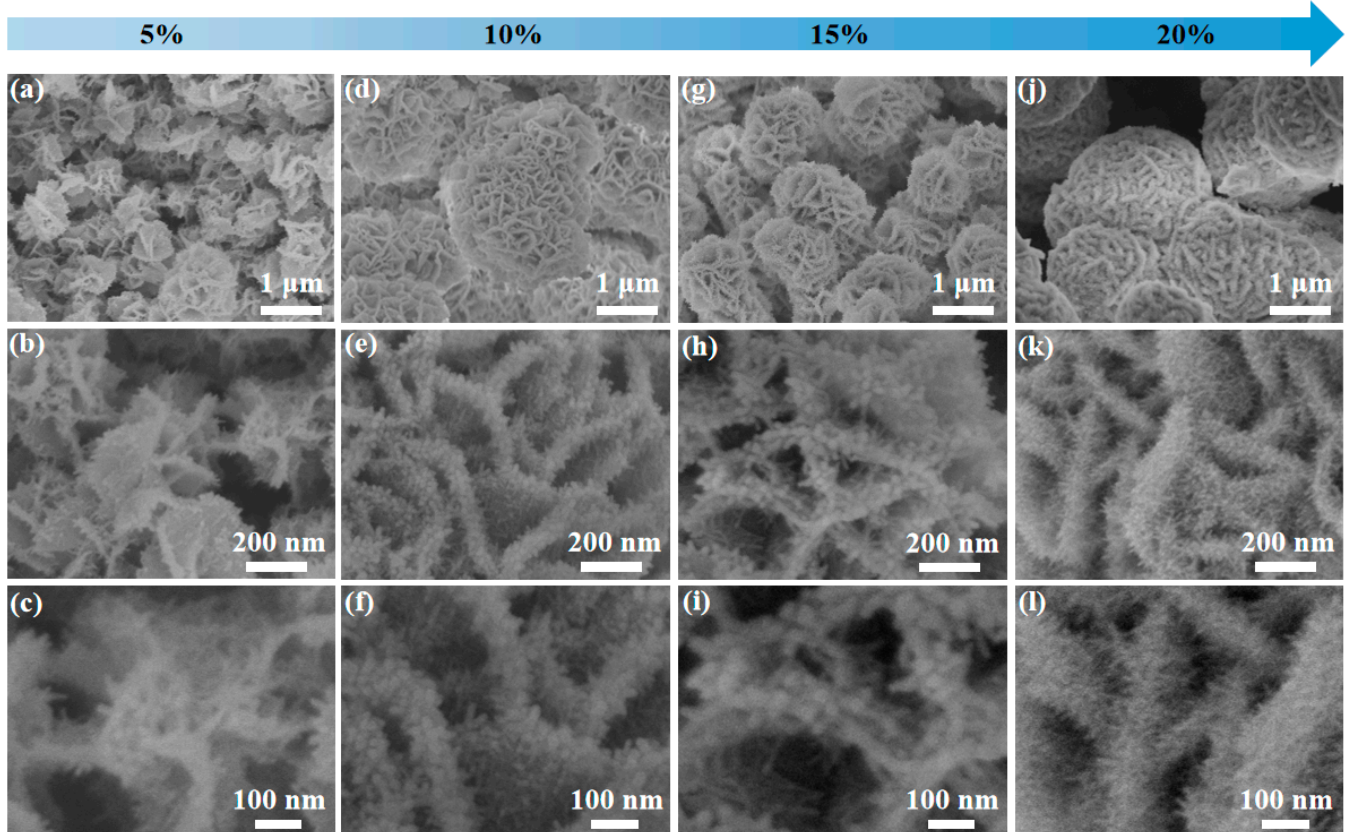


Figure 1. The SEM images of the as-prepared samples. (a–c) 5% NiS-Cu₂S-CF composites, (d–f) 10% NiS-Cu₂S-CF composites, (g–i) 15% NiS-Cu₂S-CF composites, and (j–l) 20% NiS-Cu₂S-CF composites.

The transmission electron microscopy (TEM) result presents the NiS-Cu₂S composites with a flake structure (Figure 2a). The enlarged TEM image (Figure 2b) exhibits the surface of the Cu₂S decorated with many NiS nanoneedles. The high-resolution TEM (HRTEM) image displays the two distinctive types of lattice fringes with the neighboring distance of 0.20 and 0.24 nm (Figure 2c), which correspond to the (601) facet of Cu₂S and (220) plane of NiS, respectively. Furthermore, these two lattice fringes are well-connected, indicating that the high-quality heterostructure was formed between NiS and Cu₂S, resulting in a significant improvement in the structural stability of the catalysts [25,26]. This is due to the following reasons: (1) the formed heterostructure can significantly increase the ion transfer rate between NiS and Cu₂S; (2) the NiS nanoneedles grown on Cu₂S reduce the ion-transfer distance between electrolyte and electrode, and reduce the corrosion time of the sample during the OER process, and improve the structural stability [27]. The energy-dispersive X-ray spectroscopy (EDS) elemental mappings of the 15% NiS-Cu₂S-CF and other samples (5, 10, and 20% NiS-Cu₂S-CF) are shown in Figure 2d–h and Figures S4–S6 (Supporting Materials), indicating that Cu, Ni, and S elements are uniformly distributed in the fabricated electrocatalysts.

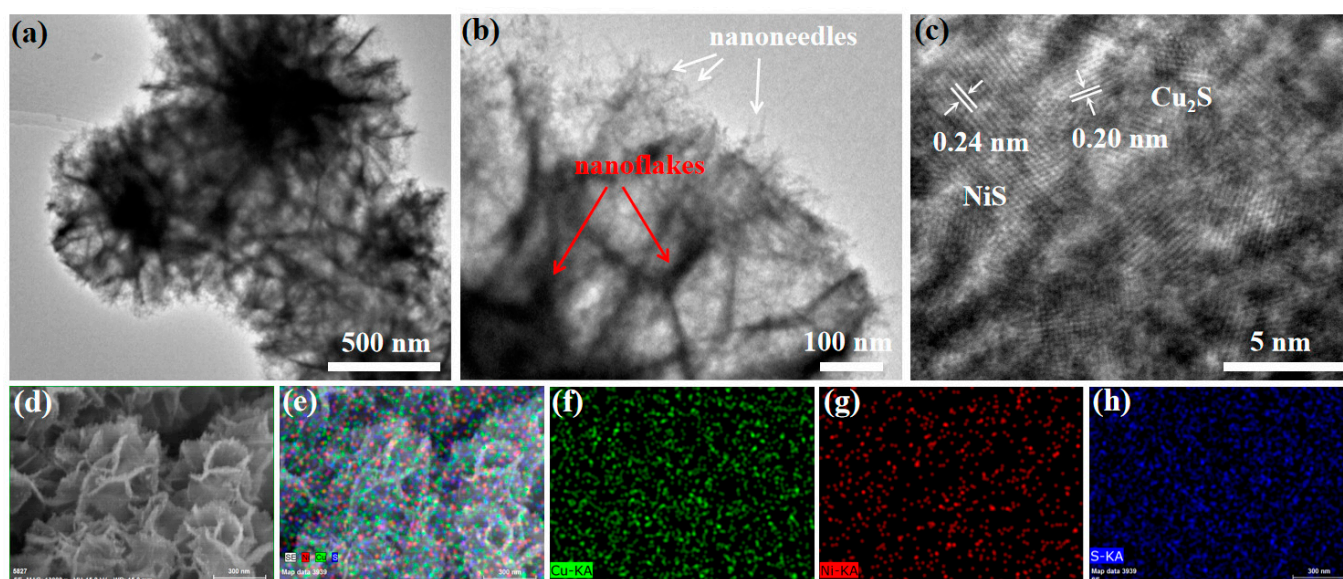


Figure 2. (a,b) TEM and (c) HRTEM images of the 15% NiS-Cu₂S-CF composites. (d–h) EDS mappings of the 15% NiS-Cu₂S-CF composites verifying the presence of Cu, Ni, and S elements.

Figure 3a,b show the X-ray diffractometry (XRD) patterns of the as-prepared products. As displayed in Figure 3a, for Cu₂S-CF composites, two peaks at 36.75° and 46.50° belong to the (0111) and (601) planes of the Cu₂S (JCPDS No. 12-0227) [28]. For NiS-CF composites, two peaks at 37.79° and 48.95° can be assigned to the (220) and (131) planes of NiS (JCPDS No. 02-1443) [29]. Furthermore, the CF substrate presents three diffraction peaks at 43.90°, 50.95°, and 74.61°. It should be noted that, with the increase in the amount of the Ni ions, the peak's intensity of the (220) and (131) of the NiS becomes increased, which suggests the large amount of NiS was successfully grown on the Cu₂S. Furthermore, the chemical composition and electronic interaction of the samples were measured by X-ray photoelectron spectroscopy (XPS). Figure 3c displays the full XPS spectra of 15% NiS-Cu₂S-CF composites, indicating the presence of S, Cu, and Ni elements. The XPS spectra of Cu 2p in NiS-Cu₂S-CF (Figure 3d) display two peaks at 932.4 and 952.2 eV along with two satellite peaks corresponding to the Cu⁰ 2p_{3/2}, Cu⁺ 2p_{3/2}, Cu⁰ 2p_{1/2}, and Cu⁺ 2p_{1/2}, respectively [30]. In addition, the XPS spectra of Ni 2p in NiS-Cu₂S-CF (Figure 3e) show two peaks at 856.1 (Ni²⁺ 2p_{3/2}) and 873.8 eV (Ni²⁺ 2p_{1/2}) along with two satellite peaks at 862.8 and 881.3 eV [31]. Moreover, the Ni(OH)₂ (863.92 and 881.52 eV) and NiO (867.36 eV) peaks were observed, confirming the oxidation state of the NiS. Compared to Cu₂S-CF and NiS-CF, the Cu 2p and Ni 2p of 15% NiS-Cu₂S-CF show positive and negative shifts, respectively, confirming the electronic interaction between NiS and Cu₂S. Furthermore, such shifts in the Cu and Ni spectra revealed strong interfacial electron transfer from Cu₂S to NiS caused by the high electronegativity of Ni atoms [32]. It should be noted that such unique electronic interactions will promote the charge transfer between NiS and Cu₂S and increase the OER performance [33]. The S 2p spectra of the NiS-Cu₂S-CF, Cu₂S-CF, and NiS-CF are shown in Figure 3f and Figure S7 (Supporting Materials), which confirm the presence of S ions in the fabricated samples [34,35]. In addition, the XPS of 5, 10, and 20% NiS-Cu₂S-CF composites are presented in Figures S8–S10 in Supporting Materials, which also confirm the oxidation state of the NiS.

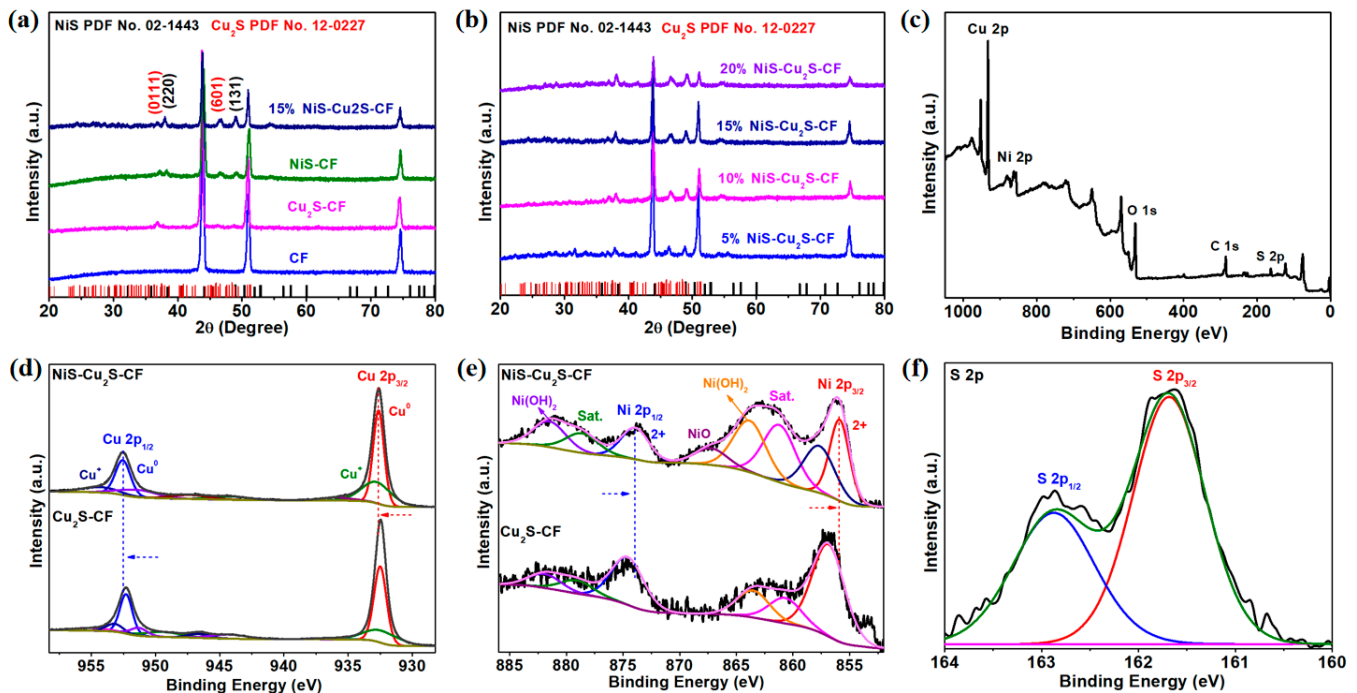


Figure 3. (a,b) XRD patterns of the as-prepared electrocatalysts. (c) The fully XPS spectra of 15% NiS-Cu₂S-CF composites. (d) high-resolution XPS spectra of Cu 2p in NiS-Cu₂S-CF and Cu₂S-CF. (e) high-resolution XPS spectra of Ni 2p in NiS-Cu₂S-CF and NiS-CF. (f) high-resolution XPS spectra of S 2p in NiS-Cu₂S-CF.

We employed the as-prepared NiS-Cu₂S-CF composites as the electrocatalyst for oxygen evolution in 1 M KOH electrolyte. Figure 4a and Figure S11 (Supporting Materials) show the linear sweep voltammetry (LSV) curves of the prepared samples. As demonstrated, the 15% NiS-Cu₂S-CF composite shows superior OER activity to those of pure CF, RuO₂, and other NiS-Cu₂S-CF composites. Figure 4b presents the overpotentials of the as-prepared samples at the current density of 20 mA cm⁻². Note that the 15% NiS-Cu₂S-CF composite showed a small overpotential of 308 mV at 20 mA cm⁻². Furthermore, the overpotential of the 15% NiS-Cu₂S-CF composite (~420 mV) was smaller than that of RuO₂ (455 mV) when the current density reached up to 50 mA cm⁻². The superior catalytic activity could be attributed to the following reasons: (1) the unique morphology can provide more ion-transfer pathways; (2) the NiS nanoneedles can provide ample reaction active sites; (3) the Cu₂S with high conductivity can promote the charge transfer ability; and (4) the synergistic effect between NiS and Cu₂S will increase the catalytic property. In addition, the overpotential of the 15% NiS-Cu₂S-CF composite was much lower than those previously reported (Table 1) [10,12,13,15,22–24,36–39], suggesting that the as-fabricated NiS-Cu₂S-CF composite is a promising OER electrocatalyst. Figure 4c shows the Tafel slopes of the as-prepared electrocatalysts. The Tafel slopes of RuO₂, NiS-CF, Cu₂S-CF, 5% NiS-Cu₂S-CF, 10% NiS-Cu₂S-CF, 15% NiS-Cu₂S-CF, and 20% NiS-Cu₂S-CF are approximately 142, 340, 286, 258, 193, 125, and 232 mV dec⁻¹, respectively. The 15% NiS-Cu₂S-CF composite shows a lower value of the Tafel slope, indicating that it has rapid catalytic kinetics during the OER process [40]. It is widely accepted that the electrochemically active surface area has an important effect on the OER. Hence, the cyclic voltammetry (CV) curve was taken to assess the electrochemical double-layer capacitance (C_{dl}) of the samples. The CV curves at various scan rates of the as-prepared samples are shown in Figure S12 (Supporting Materials). The calculated C_{dl} of the samples is shown in Figure 4d, and the C_{dl} values of 5% NiS-Cu₂S-CF, 10% NiS-Cu₂S-CF, 15% NiS-Cu₂S-CF, and 20% NiS-Cu₂S-CF are approximately 60, 102, 153, and 89 mF cm⁻², respectively. The 15% NiS-Cu₂S-CF has the highest value of the C_{dl} , demonstrating that it can provide more catalytic active sites during the OER process [41,42].

The electrochemical impedance spectroscopy (EIS) was performed at the potential of 1.51 V vs. reversible hydrogen electrode (RHE) to investigate the charge transfer performance of the samples. Figure 4e presents the EIS spectra and the equivalent circuit (the inset of Figure 4e) of the samples, indicating that the charge-transfer resistance (R_{ct}) of NiS-CF, Cu₂S-CF, 5% NiS-Cu₂S-CF, 10% NiS-Cu₂S-CF, 15% NiS-Cu₂S-CF, and 20% NiS-Cu₂S-CF is 87.1, 70.3, 32.9, 24.5, 8.2, and 30.7 Ω , respectively. The 15% NiS-Cu₂S-CF composite shows a smaller R_{ct} , indicating a faster ion-transfer rate during the OER process than other samples [43–45]. The smaller R_{ct} of 15% NiS-Cu₂S-CF is due to the appropriate amount of NiS grown on CuS, which can greatly enhance the electrical conductivity, resulting in a higher charge transfer rate between the electrode and electrolyte. Moreover, we also tested the cycling stability of the 15% NiS-Cu₂S-CF composite. Figure S13 (Supporting Materials) presents the LSV curves of the 15% NiS-Cu₂S-CF composite before and after 1000 cycling tests. The LSV curves slightly changed after the 1000 cycling tests, which indicates that the 15% NiS-Cu₂S-CF composite has excellent cycling catalytic activity. Figures S14 and S15 (Supporting Materials) show the SEM and XPS results of the 15% NiS-Cu₂S-CF composite after 1000 cycling tests. The SEM image indicates that the 15% NiS-Cu₂S-CF composite shows no appreciable structure change compared to before the cycling test. The XPS results indicate the presence of a metal-oxygen (M-O) bond after 1000 cycling tests (Figure S15e), indicating that 15% NiS-Cu₂S-CF was oxidated during the cycling tests. Furthermore, the long-term cycling stability of the 15% NiS-Cu₂S-CF and RuO₂ was measured using the amperometric $i-t$ curve at a potential of 1.53 V vs. RHE. As shown in Figure 4f, even tested for 30 h, the 15% NiS-Cu₂S-CF composite still shows a remarkable OER activity than RuO₂. This result confirms that our NiS-Cu₂S-CF composite is a stable and cost-effective electrocatalyst for OER.

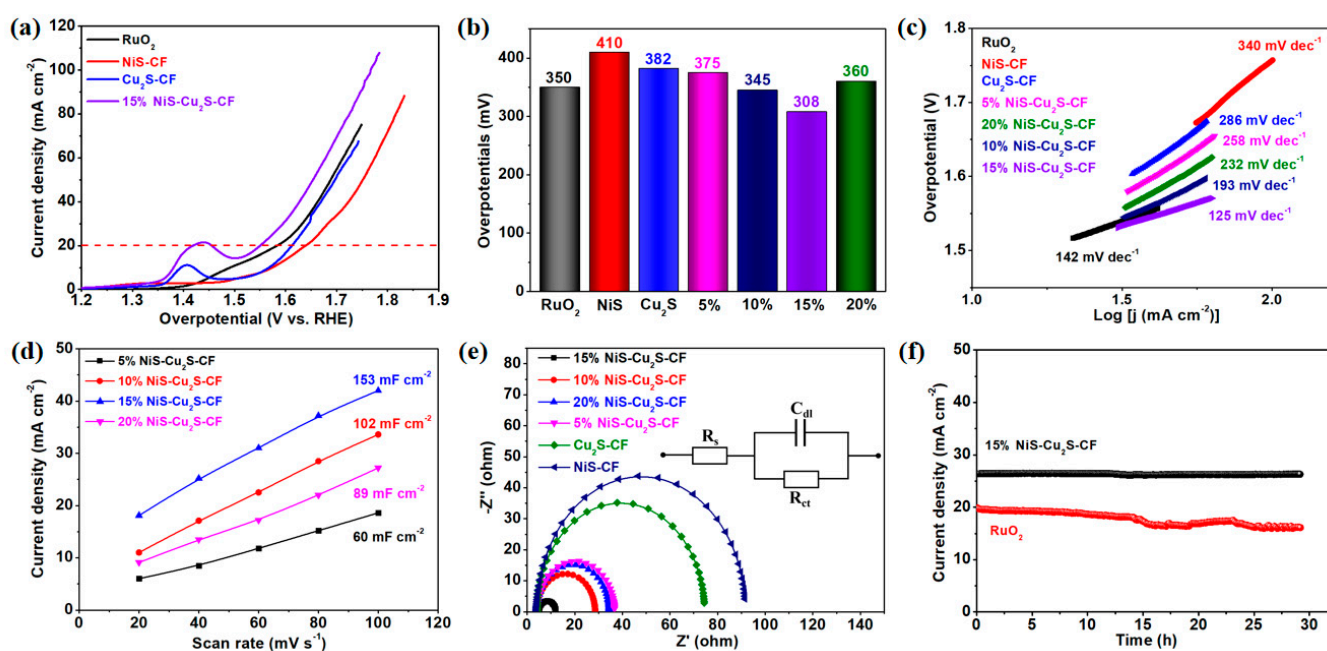


Figure 4. (a) LSV curves of the RuO₂, NiS-CF, Cu₂S-CF, and 15% NiS-Cu₂S-CF. (b) The overpotentials of the as-fabricated samples at the current density of 20 mA cm⁻². (c) TF slope of the as-fabricated samples. (d) C_{dl} of the as-fabricated samples. (e) EIS of the as-fabricated samples (the inset shows the equivalent circuit). (f) Long-term cycling stability of 15% NiS-Cu₂S-CF and RuO₂.

Table 1. Comparison of the electrocatalytic activity of the metal sulfide-based electrocatalysts for OER.

Electrocatalysts	Overpotential (mV)	Current Density (mA cm ⁻²)	Ref.
15% NiS-Cu ₂ S-CF	308	20	This work
Cu ₂ S-CF	336	20	[10]
CuS-CC	358	10	[12]
Cu ₂ S-Ni(OH) ₂	500	10	[13]
Cu ₂ S-CuO	380	10	[15]
NiS-Bi ₂ WO ₆	527	10	[22]
NiS-C ₃ N ₄	334	10	[23]
NiS-Fe ₃ O ₄	310	10	[24]
NiS-Fe ₃ S ₄	338	10	[36]
NiS _x -Fe ₃ O ₄ -rGO	330	10	[37]
Cu ₉ S ₅ -Ni foam	301	10	[38]
3% Ni-doped CuS	390	10	[39]

4. Conclusions

In conclusion, the NiS-Cu₂S-CF composites with a unique morphology were successfully prepared using a facile method. The optimized 15% NiS-Cu₂S-CF electrocatalyst exhibited a lower overpotential of 308 mV at 20 mA cm⁻² for OER than that of noble-metal-based electrocatalysts, and those metal sulfides reported previously. The composite's remarkable catalytic performance is attributed to (1) its unique morphology that provides not only more reaction active sites but also more ion-transfer pathways; (2) improved conductivity and enhanced structural stability of the formed NiS-Cu₂S heterostructure; (3) increased electron transfer property owing to the synergistic effect between NiS and Cu₂S. This work demonstrates that the NiS-Cu₂S-CF composite is a potential candidate for high-performance oxygen evolution.

Supplementary Materials: The following supporting information can be downloaded at: <https://www.mdpi.com/article/10.3390/mi13020278/s1>, fabrication of electrocatalysts on copper foam, materials, and electrochemical characterizations, Table S1: Molar ratios of Ni and Cu ions in the NiS-Cu₂S-CF composites; Figure S1: SEM images of the (a) CF and (b) Cu₂O-CF composites; Figure S2: SEM images of the Cu₂S-CF composites; Figure S3: SEM images of the NiS-CF composites; Figure S4: The S XPS spectra of the (a) Cu₂S-CF and (b) NiS-CF composites; Figure S5: LSV curves of the 5% NiS-Cu₂S-CF, 10% NiS-Cu₂S-CF, and 20% NiS-Cu₂S-CF composites; Figure S6: CV curves of the (a) 5% NiS-Cu₂S-CF composites, (b) 10% NiS-Cu₂S-CF composites, (c) 15% NiS-Cu₂S-CF composites, and (d) 20% NiS-Cu₂S-CF composites; Figure S7: LSV curves of the 15% NiS-Cu₂S-CF composites after 1000 cycles test; Figure S8: SEM images of the 15% NiS-Cu₂S-CF composites after 1000 cycles test; Figure S9: XPS of the 15% NiS-Cu₂S-CF composites after 1000 cycles test. (a) Fully XPS spectra, (b) Cu 2p, (c) Ni 2p, (d) S 2p, and (e) O 1s.

Author Contributions: Conceptualization, L.W. and M.L.; methodology, Y.L. and J.L.; software, L.W.; writing—original draft preparation, J.D. and D.J.K.; writing—review and editing. All authors have read and agreed to the published version of the manuscript.

Funding: This work was supported by the National Natural Science Foundation of China (21273010), Program for Natural Science of Henan Province (162300410004), Key Scientific Research Projects of Henan Universities (19A150014), and Anyang Normal University College Student Innovation Fund Project (ASCX/2018-Z044). Y. Qian and D J Kang also thank the BioNano Health-Guard Research Center funded by the Ministry of Science, ICT & Future Planning of Korea as Global Frontier Project (H-GUARD_2014M3A6B2060521).

Data Availability Statement: All data needed to evaluate the conclusions in the paper are present in the paper and/or the Supplementary Materials. Additional data related to this paper may be requested from the authors.

Conflicts of Interest: The authors declare no conflict of interest.

References

1. Kuo, D.Y.; Kawasaki, J.K.; Nelson, J.N.; Kloppenburg, J.; Hautier, G.; Shen, K.M.; Schlom, D.G.; Suntivich, J. Influence of surface adsorption on the oxygen evolution reaction on IrO₂(110). *J. Am. Chem. Soc.* **2017**, *139*, 3473–3479. [[CrossRef](#)] [[PubMed](#)]
2. Stoerzinger, K.A.; Diaz-Morales, O.; Kolb, M.; Rao, R.R.; Frydendal, R.; Qiao, L.; Wang, X.R.; Halck, N.B.; Rossmeisl, J.; Hansen, H.A.; et al. Orientation-dependent oxygen evolution on RuO₂ without lattice exchange. *ACS Energy Lett.* **2017**, *2*, 876–881. [[CrossRef](#)]
3. Cai, P.; Huang, J.; Chen, J.; Wen, Z. Oxygen-containing amorphous cobalt sulfide porous nanocubes as high-activity electrocatalysts for the oxygen evolution reaction in an alkaline/neutral medium. *Angew. Chem.* **2017**, *56*, 4858–4861. [[CrossRef](#)] [[PubMed](#)]
4. Wu, Z.P.; Lu, X.F.; Zang, S.Q.; Lou, X.W. Non-noble-metal-based electrocatalysts toward the oxygen evolution reaction. *Adv. Funct. Mater.* **2020**, *30*, 1910274. [[CrossRef](#)]
5. Peng, L.; Shah, S.S.A.; Wei, Z. Recent developments in metal phosphide and sulfide electrocatalysts for oxygen evolution reaction. *Chin. J. Catal.* **2018**, *39*, 1575–1593. [[CrossRef](#)]
6. Cui, M.; Yang, C.; Li, B.; Dong, Q.; Wu, M.; Hwang, S.; Xie, H.; Wang, X.; Wang, G.; Hu, L. High-entropy metal sulfide nanoparticles promise high-performance oxygen evolution reaction. *Adv. Energy Mater.* **2020**, *11*, 2002887. [[CrossRef](#)]
7. Thangasamy, P.; Oh, S.; Nam, S.; Randriamahazaka, H.; Oh, I.K. Ferrocene-incorporated cobalt sulfide nanoarchitecture for superior oxygen evolution reaction. *Small* **2020**, *16*, 2001665. [[CrossRef](#)]
8. Pujari, R.B.; Gund, G.S.; Patil, S.J.; Park, H.S.; Lee, D.W. Anion-exchange phase control of manganese sulfide for oxygen evolution reaction. *J. Mater. Chem. A* **2020**, *8*, 3901–3909. [[CrossRef](#)]
9. Li, Y.; Zhang, X.; Zhuo, S.; Liu, S.; Han, A.; Li, L.; Tian, Y. Flower-like CoO@Cu₂S nanocomposite for enhanced oxygen evolution reaction. *Appl. Surf. Sci.* **2021**, *555*, 149441. [[CrossRef](#)]
10. He, L.; Zhou, D.; Lin, Y.; Ge, R.; Hou, X.; Sun, X.; Zheng, C. Ultrarapid in situ synthesis of Cu₂S nanosheet arrays on copper foam with room-temperature-active iodine plasma for efficient and cost-effective oxygen evolution. *ACS Catal.* **2018**, *8*, 3859–3864. [[CrossRef](#)]
11. Deng, S.; Shen, Y.; Xie, D.; Lu, Y.; Yu, X.; Yang, L.; Wang, X.; Xia, X.; Tu, J. Directional construction of Cu₂S branch arrays for advanced oxygen evolution reaction. *J. Energy Chem.* **2019**, *39*, 61–67. [[CrossRef](#)]
12. Li, K.; Qian, Y.; Zhang, H.; Zhang, L.; Chai, Q.; Wang, Q.; Du, J.; Han, Y.; Wang, W.; Kang, D.J. Highly efficient oxygen evolution electrocatalysts based on nanosheet-shaped CuS in situ grown on carbon cloth. *Ceram. Int.* **2019**, *45*, 10664–10671. [[CrossRef](#)]
13. Yang, D.; Gao, L.; Yang, J.H. Facile synthesis of ultrathin Ni(OH)₂-Cu₂S hexagonal nanosheets hybrid for oxygen evolution reaction. *J. Power Sources* **2017**, *359*, 52–56. [[CrossRef](#)]
14. Guan, X.; Sun, X.; Feng, H.; Zhang, J.; Wen, H.; Tian, W.; Zheng, D.; Yao, Y. Rational interface engineering of Cu₂S-CoO_x/CF enhances oxygen evolution reaction activity. *Chem. Commun.* **2020**, *56*, 13571–13574. [[CrossRef](#)]
15. Zuo, Y.; Liu, Y.; Li, J.; Du, R.; Han, X.; Zhang, T.; Arbiol, J.; Divins, N.J.; Llorca, J.; Guisjarro, N.; et al. In situ electrochemical oxidation of Cu₂S into CuO nanowires as a durable and efficient electrocatalyst for oxygen evolution reaction. *Chem. Mater.* **2019**, *31*, 7732–7743. [[CrossRef](#)]
16. Ding, X.; Li, W.; Kuang, H.; Qu, M.; Cui, M.; Zhao, C.; Qi, D.C.; Oropeza, F.E.; Zhang, K.H.L. An Fe stabilized metallic phase of NiS₂ for the highly efficient oxygen evolution reaction. *Nanoscale* **2019**, *11*, 23217–23225. [[CrossRef](#)]
17. Khan, N.A.; Rashid, N.; Junaid, M.; Zafar, M.N.; Faheem, M.; Ahmad, I. NiO/NiS heterostructures: An efficient and stable electrocatalyst for oxygen evolution reaction. *ACS Appl. Energy Mater.* **2019**, *2*, 3587–3594. [[CrossRef](#)]
18. Xue, Z.; Li, X.; Liu, Q.; Cai, M.; Liu, K.; Liu, M.; Ke, Z.; Liu, X.; Li, G. Interfacial electronic structure modulation of NiTe nanoarrays with NiS nanodots facilitates electrocatalytic oxygen evolution. *Adv. Mater.* **2019**, *31*, 1900430. [[CrossRef](#)]
19. Wang, L.; Qian, Y.; Du, J.; Wu, H.; Wang, Z.; Li, G.; Li, K.; Wang, W.; Kang, D.J. Facile synthesis of cactus-shaped CdS-Cu₉S₅ heterostructure on copper foam with enhanced photoelectrochemical performance. *Appl. Surf. Sci.* **2019**, *492*, 849–855. [[CrossRef](#)]
20. Zhang, Z.; Zhu, H.; Hao, J.; Lu, S.; Duan, F.; Xu, F.; Du, M. One-dimensional, space-confined, solid-phase growth of the Cu₉S₅@MoS₂ core-shell heterostructure for electrocatalytic hydrogen evolution. *J. Colloid Interface Sci.* **2021**, *595*, 88–97. [[CrossRef](#)]
21. Zhang, S.; Li, Y.; Zhu, H.; Lu, S.; Ma, P.; Dong, W.; Duan, F.; Chen, M.; Du, M. Understanding the role of nanoscale heterointerfaces in core/shell structures for water splitting: Covalent bonding interaction boosts the activity of binary transition-metal sulfides. *ACS Appl. Mater. Interfaces* **2020**, *12*, 6250–6261. [[CrossRef](#)] [[PubMed](#)]
22. Li, J.; Xu, X.; Zhang, B.; Hou, W.; Lv, S.; Shi, Y. Controlled synthesis and fine-tuned interface of NiS nanoparticles/Bi₂WO₆ nanosheets heterogeneous as electrocatalyst for oxygen evolution reaction. *Appl. Surf. Sci.* **2020**, *526*, 146718. [[CrossRef](#)]
23. Luo, Y.; Qin, J.; Yang, G.; Luo, S.; Zhao, Z.; Chen, M.; Ma, J. N-Ni-S coordination sites of NiS/C₃N₄ formed by an electrochemical-pyrolysis strategy for boosting oxygen evolution reaction. *Chem. Eng. J.* **2021**, *410*, 128394. [[CrossRef](#)]
24. Jiang, S.; Shao, H.; Cao, G.; Li, H.; Xu, W.; Li, J.; Fang, J.; Wang, X. Waste cotton fabric derived porous carbon containing Fe₃O₄/NiS nanoparticles for electrocatalytic oxygen evolution. *J. Mater. Sci. Technol.* **2020**, *59*, 92–99. [[CrossRef](#)]
25. Jia, Q.; Wang, X.; Wei, S.; Zhou, C.; Wang, J.; Liu, J. Porous flower-like Mo-doped NiS heterostructure as highly efficient and robust electrocatalyst for overall water splitting. *Appl. Surf. Sci.* **2019**, *484*, 1052–1060. [[CrossRef](#)]
26. Li, M.; Qian, Y.; Du, J.; Wu, H.; Zhang, L.; Li, G.; Li, K.; Wang, W.; Kang, D.J. CuS nanosheets decorated with CoS₂ nanoparticles as an efficient electrocatalyst for enhanced hydrogen evolution at all pH values. *ACS Sustain. Chem. Eng.* **2019**, *7*, 14016–14022. [[CrossRef](#)]

27. Zhang, F.; Wang, L.; Park, M.; Song, K.; Choi, H.; Shi, H.; Lee, H.J.; Pang, H. Nickel sulfide nanorods decorated on graphene as advanced hydrogen evolution electrocatalysts in acidic and alkaline media. *J. Colloid Interface Sci.* **2022**, *608*, 2633–2640. [[CrossRef](#)]
28. Ni, S.; Lv, X.; Li, T.; Yang, X. Fabrication of Cu₂S cathode for Li-ion battery via a low temperature dry thermal sulfuration method. *Mater. Chem. Phys.* **2013**, *143*, 349–354. [[CrossRef](#)]
29. Dong, Y.; Wu, R.; Jiang, P.; Wang, G.; Chen, Y.; Wu, X.; Zhang, C. Efficient photoelectrochemical hydrogen generation from water using a robust photocathode formed by CdTe QDs and nickel ion. *ACS Sustain. Chem. Eng.* **2015**, *3*, 2429–2434. [[CrossRef](#)]
30. Zhang, J.; Li, W.; Li, Y.; Zhong, L.; Xu, C. Self-optimizing bifunctional CdS/Cu₂S with coexistence of light-reduced CuO for highly efficient photocatalytic H₂ generation under visible-light irradiation. *Appl. Catal. B Environ.* **2017**, *217*, 30–36. [[CrossRef](#)]
31. Guan, B.; Li, Y.; Yin, B.; Liu, K.; Wang, D.; Zhang, H.; Cheng, C. Synthesis of hierarchical NiS microflowers for high performance asymmetric supercapacitor. *Chem. Eng. J.* **2017**, *308*, 1165–1173. [[CrossRef](#)]
32. Liu, P.; Yan, J.; Mao, J.; Li, J.; Liang, D.; Song, W. In-plane intergrowth CoS₂/MoS₂ nanosheets: Binary metal–organic framework evolution and efficient alkaline HER electrocatalysis. *J. Mater. Chem. A* **2020**, *8*, 11435–11441. [[CrossRef](#)]
33. Qian, Y.; Yu, J.; Zhang, Y.; Zhang, F.; Su, C.; Shi, H.; Kang, D.J.; Pang, H. Interfacial microenvironment modulation enhancing catalytic kinetics of binary metal sulfides heterostructures for advanced water splitting electrocatalysts. *Small Methods* **2022**, *6*, 2101186. [[CrossRef](#)] [[PubMed](#)]
34. Chen, Z.; Yang, S.; Tian, Z.; Zhu, B. NiS and graphene as dual cocatalysts for the enhanced photocatalytic H₂ production activity of g-C₃N₄. *Appl. Surf. Sci.* **2019**, *469*, 657–665. [[CrossRef](#)]
35. Qian, Y.; Yu, J.; Zhang, F.; Kang, Y.; Su, C.; Pang, H. Facile synthesis of sub-10 nm ZnS/ZnO nanoflakes for high-performance flexible triboelectric nanogenerators. *Nano Energy* **2021**, *88*, 106256. [[CrossRef](#)]
36. Hao, Z.; Wei, P.; Kang, H.; Yang, Y.; Li, J.; Chen, X.; Guo, D.; Liu, L. Three-dimensional Fe₃S₄@NiS hollow nanospheres as efficient electrocatalysts for oxygen evolution reaction. *J. Electroanal. Chem.* **2019**, *850*, 113436. [[CrossRef](#)]
37. Zhu, G.; Xie, X.; Liu, Y.; Li, X.; Xu, K.; Shen, X.; Yao, Y.; Shah, S.A. Fe₃O₄@NiS_x/rGO composites with amounts of heterointerfaces and enhanced electrocatalytic properties for oxygen evolution. *Appl. Surf. Sci.* **2018**, *442*, 256–263. [[CrossRef](#)]
38. Chakraborty, B.; Kalra, S.; Beltran-Suito, R.; Das, C.; Hellmann, T.; Menezes, P.W.; Driess, M. A Low-temperature molecular precursor approach to copper-based nano-sized digenite mineral for efficient electrocatalytic oxygen evolution reaction. *Chem. Asian J.* **2020**, *15*, 852–859. [[CrossRef](#)]
39. Kundu, J.; Khilari, S.; Bhunia, K.; Pradhan, D. Ni-doped CuS as an efficient electrocatalyst for the oxygen evolution reaction. *Catal. Sci. Technol.* **2019**, *9*, 406–417. [[CrossRef](#)]
40. Zhao, G.; Li, P.; Cheng, N.; Dou, S.X.; Sun, W. An Ir/Ni(OH)₂ heterostructured electrocatalyst for the oxygen evolution reaction: Breaking the scaling relation, stabilizing iridium(V), and beyond. *Adv. Mater.* **2020**, *32*, 2000872. [[CrossRef](#)]
41. Zhang, S.; Xue, H.; Li, W.L.; Sun, J.; Guo, N.; Song, T.; Dong, H.; Zhang, J.; Ge, X.; Zhang, W.; et al. Constructing precise coordination of nickel active sites on hierarchical porous carbon framework for superior oxygen reduction. *Small* **2021**, *17*, 2102125. [[CrossRef](#)] [[PubMed](#)]
42. Bai, X.J.; Lu, X.Y.; Ju, R.; Chen, H.; Shao, L.; Zhai, X.; Li, Y.N.; Fan, F.Q.; Fu, Y.; Qi, W. Preparation of MOF film/aerogel composite catalysts via substrate-seeding secondary-growth for the oxygen evolution reaction and CO₂ cycloaddition. *Angew. Chem.* **2021**, *60*, 701–705. [[CrossRef](#)] [[PubMed](#)]
43. Zhang, F.; Eom, T.; Cho, M.; Lee, H.J.; Pang, H. Fabrication of defect-rich bifunctional hollow NiTe₂ nanotubes for high performance hydrogen evolution electrocatalysts and supercapacitors. *J. Energy Storage* **2021**, *42*, 103098. [[CrossRef](#)]
44. Qian, Y.; Du, J.; Kang, D.J. Enhanced electrochemical performance of porous Co-doped TiO₂ nanomaterials prepared by a solvothermal method. *Microporous Mesoporous Mater.* **2019**, *273*, 148–155. [[CrossRef](#)]
45. Zheng, F.; Zhang, W.; Zhang, X.; Zhang, Y.; Chen, W. Sub-2 nm ultrathin and robust 2D FeNi layered double hydroxide nanosheets packed with 1D FeNi-MOFs for enhanced oxygen evolution electrocatalysis. *Adv. Funct. Mater.* **2021**, *31*, 2103318. [[CrossRef](#)]